Kobe University Repository : Kernel

PDF issue: 2025-12-05

Adhesive interphase analyses of isotactic polypropylene and cyanoacrylate with cobalt complex primers

Matsumoto, Takuya ; Nakanishi, Yuta ; Hongo, Chizuru ; Hakukawa, Hideki ; Horiuchi, Shin ; Nishino, Takashi

(Citation)
Polymer,137:63-71

(Issue Date)
2018-02-14

(Resource Type)
journal article

(Version)
Accepted Manuscript

(Rights)
© 2018 Elsevier Ltd.
This manuscript version is made available under the CC-BY-NC-ND 4.0 license
http://creativecommons.org/licenses/by-nc-nd/4.0/

(URL)
https://hdl.handle.net/20.500.14094/90004796

KOBE UNIVERSITY

Adhesive Interphase Analyses of *Isotactic* Polypropylene and Cyanoacrylate with Cobalt Complex Primers

Takuya Matsumoto[a], *Yuta Nakanishi*[a], *Chizuru Hongo*[a], *Hideki Hakukawa*[b], *Shin Horiuchi*[b], *Takashi Nishino**[a]

[a] Department of Chemical Science and Engineering, Graduate School of Engineering, Kobe University, Rokko, Nada, Kobe, 657-8501, Japan

[b] Research Laboratory for Adhesion and Interfacial Phenomena, Nanotechnology Research Institute, National Institute of Advanced Industrial Science and Technology (AIST), 1-1-1, Higashi, Tsukuba, Ibaraki 305-8565, Japan

Key Words

Adhesive interphase, Polypropylene, Cobalt acetylacetonate, Confocal nano-Raman scattering microscopy, Scanning transmission electron microscopy with energy dispersive X-ray spectroscopy

ABSTRACT

The modification of surface properties of *isotactic* polypropylene (*it*.PP) has attracted much attention in fundamental science and industrial applications. Primer treatment is a promising methods that is employed to overcome the poor adhesive property of *it*.PP. In this study, we examined the primer effect of the cobalt complexes, cobalt (II) acetylacetonate $Co(acac)_2$ and cobalt (III) acetylacetonate $Co(acac)_3$, from the perspectives of adhesive strength, curing process, surface structure, affinity between substrate and adhesive, morphology and interfacial thickness. The results obtained explain the increased adhesive strength between an *isotactic* polypropylene substrate and a cyanoacrylate adhesive. In particular, the interfacial regions were evaluated as "interphase" by nano-Raman scattering microscopy and transmission electron microscope-energy-dispersive X-ray spectroscopy. The region is expanded by applying $Co(acac)_2$ primer as the adhesive strength increased. The $Co(acac)_2$ primer caused the increased adhesive property with the enhancement of molecular interaction, chemical affinity, and mutual diffusion.

Introduction

Since achieving the polymerization of α-olefins by Ziegler–Natta catalysts in 1950s,[1,2] poly-α-olefins, in particular *isotactic* polypropylene (*it.*PP), have been widely employed in daily life, architecture, and industrial fields.[3] The molecular weight, regioregularity, tacticity, and copolymerization segment of poly-α-olefins are readily controlled by the polymerization condition, and poly-α-olefins with various mechanical, thermal and optical properties have been reported.[4–7] The many advantages of *it.*PP, such as lightweight, processability, thermal stability, chemical resistance, and low hygroscopicity, have accelerated its widespread acceptance compared to other thermoplastic resins.[3,8] In addition, their properties have been modified drastically by blending with other polymers, laminating and adding inorganic fillers and fibers.[8–13] Therefore, *it.*PP is included not only in packages and electrical appliances but also in building roofs and automotive frames. *It.*PP has received much attentions as an alternative to metallic materials in automobiles, and it is expected that further development for this application will lead to their reduced weight and an improved fuel efficiency for energy saving.[14,15]

However, the poor adhesion of *it.*PP is well known as one of disadvantages,[16,17] and originates from its high crystallinity and low reactive chemical structure without any polar substituents. In contrast, from the perspectives of the complexity of the many component materials in the vehicles, the adhesion of *it.*PP with polymers, carbon fibers, or metals is a significant challenge. In order to improve the adhesive properties, various surface modification methods of *it.*PP have been proposed.[17–24] In general, there are both physical and chemical treatments. Physical treatments include blast, frame, UV, plasma, and corona discharge, while chromate and primer treatments are classified as chemical treatment. Primer treatment involves the application of primers to *it.*PP substrates before adhering, and it promotes the adhesiveness of the *it.*PP

surface.[25–28] Kimura *et al.* reported on the primer effect of metallic acetylacetonates for the modification of adhesion properties between polyolefins and cyanoacrylate (CA) adhesives.[18, 28–30] Sonnenschein *et al.* reported that trialkyl boranes performed as primers for the surface modification of polyolefins.[31,32]

In this way, several primers for the improvement of the adhesion of *it*.PP substrates have been examined and clarified,[25–28] but there is a limited variety of primers, and there is to date no detailed understanding of the mechanism of the primer effect on the adhesion interphase. The investigation of the interphase is a significant challenge because adhesion is a complicated phenomenon that exists within a limited spatial space. In this study, the term “interphase” is used as an alternative to “interface”, which is generally accepted. However, as described below, we propose that the adhesive region has a finite thickness, and the term “interphase” is more appropriate.[33–36] Adhesion involves the anchor effect, chemical bonding, electrostatic interaction, van der Waals interaction and diffusion.[16] Recently, analytical techniques and instruments have been developed for adhesion interfaces, including the Fourier transform infrared spectroscopy in attenuated total reflection method (ATR-FTIR),[37–40] energy-dispersive X-ray spectroscopy (EDX),[41,42] X-ray photoelectron spectroscopy (XPS),[37,38,43–46] secondary ion mass spectrometry (SIMS),[43,44,47] scanning near-field optical microscopy (SNOM),[48] grazing incident angle X-ray diffraction,[49] and sum frequency generation (SFG) spectroscopy[50–53]. Their extremely high spatial resolution, good detection threshold, and ability to acquire simultaneous multi-measurements have been achieved in the interfacial analyses. However, these analysis techniques also have disadvantages, including limitations with respect to the analysis subjects, time resolution and internal observation of the microstructure. To obtain a

deeper insight into the adhesive mechanism, a more detailed evaluation of the adhesion and interphase is required.

Herein, we focus on the primer effects of cobalt acetylacetonate complexes in the adhesion system of *it*.PP/CA/*it*.PP and we evaluated the adhesion interphase by performing confocal Raman scattering microscopy and transmission electron microscope-EDX (TEM-EDX). It is well known that monomer ethylcyanoacrylate in the CA adhesive is rapidly polymerized and cured by moisture under ambient atmosphere. CA adhesives are easily accessible in our daily life as well as in the field of material engineering.[29,54] In this regard, CA adhesives have significant practical advantages. Therefore, we investigated the relationship between adhesive properties and surface properties from the prespectives of the primer effect on the *it*.PP substrates, surface crystallinity of *it*.PP, chemical affinity of cobalt complexes, and the curing process.

Experiments

Materials

It.PP pellets (NOBLEN D101, MFR = 0.5 g/10 min.) were supplied from Sumitomo Chemical Industry Co. Ltd.. CA adhesive (Loctite401 (>90% ethyl cyanoacrylate, containing <10% polymethylmethacrylate)) was supplied from Henkel Co. Ltd.. Bis(2,4-pentadionato)cobalt (II) ($Co(acac)_2$) and Tris(2,4-pentadionato)cobalt (III) ($Co(acac)_3$) were purchased from TCI Co. Ltd.. Toluene and iodomethane were purchased from Nakaraitesk Co. Ltd.. Ethyl 2-cyano-2-methylpropionate was purchased from TCI Co. Ltd..

T-peel test

It.PP substrates that were around 200 μm thick were prepared for T-peel tests by the melt press of pellets at 180 °C under 6.0 MPa, followed by quenching. Cobalt complex primers (0.5 wt%) in toluene solution were spin-coated onto *it*.PP substrates (20 mm × 60 mm) using a spin coater (Micro Tech. Co. Ltd., ASS-302) with 800 rpm for 12 s. The primer concentration was optimized, as shown in Figure S12 of the Supplementary material. The primer-coated substrates were exposed into ambient atmosphere for 30 min. This period is called the “open time”. After casting CA adhesive on the substrates, other non-CA-coated substrates were overlapped on the coating side of CA-coated substrates, as shown in Figure S2 in the Supplementary material, then the adhered specimens were pressed using a 500 g weight for 2 days. The T-peel tests were carried out on the autograph (AGS-1kND, SHIMADZU Co. Ltd.) with a tensile speed of 50 mm/min. T-peel tests performed for five or more adhered specimens were prepared under the same condition.

Raman scattering measurement

Raman scattering measurements were performed on alpha300R (WITec Co. Ltd.) using a Nd/YAG laser (532 nm). The employed measurement modes were single points, line scanning and two-dimensional (2D) mapping. In the 2D mapping measurements, the mapping area was 35 μm × 35 μm. The Raman bands employed for 2D imaging were 812 cm^{-1} (ν_{CH2}, $\nu_{C\text{-}C}$, $\nu_{C\text{-}CH}$), which originated from *it.*PP[55] and 2247 cm^{-1} (ν_{CN}) of CA[56]. The lateral resolution d_{xy} is defined as shown below:

$$d_{xy} = \frac{0.51 \times \lambda}{NA} = \frac{0.51 \times 532}{0.75} = 362 \text{ (nm)}$$

where NA is the numerical aperture of objective lenses and λ is the wavelength of the laser.

To investigate the interfacial regions, the cross sections of adhered samples were first cut with razor, then embedded in epoxy resins Araldite® RAPID was obtained by curing at room temperature overnight. Next, the cross section sides of the embedded samples were milled in an abrasive machine (SBT920, Meiwafosis Co. Ltd.). The flattening of the cross-sections was performed by Ar ion polishing using a cross-section polisher (IB-09010CP CPIII, JEOL Co. Ltd.). The polishing condition was 4 kV, 70 μA for 40 h.

Investigation of curing rate of CA adhesive

The cobalt complex primers were cast on the *it.*PP substrates (10 mm × 10 mm), and the substrates were then exposed to ambient atmosphere for 30 min. After a drop of CA adhesive was cast and then two *it.*PP substrates were adhered, each adhered specimen was prepared. In the confocal Raman scattering measurement, the center of the CA layer was the focus. Raman scattering spectra were obtained every 10 s.

Scanning electron microscopy (SEM) observation

To observe the surface of the adhered side of *it*.PP substrates, we used SEM (JSM-5610LVS, JEOL Co. Ltd.) with a 10 kV electron accelerating voltage. The samples were coated with platinum.

X-ray diffraction measurement

We performed X-ray diffraction measurements on a Smart Lab (RIGAKU Co. Ltd.). The X-ray beam source was CuKα (40kV, 30 mA) and the incidence angle was 0.10°. This incidence angle was smaller than the critical angle of *it*.PP (α_c = 0.149°), where there was total reflection of the incident X-ray.[57] The diffraction profiles were obtained from out-of-plane and in-plane geometries. The X-ray diffraction originated from the structure within several nanometers from the top surface of substrates. In addition, we performed out-of-plane and in-plane measurements using a synchrotron beam (beam energy: 10 keV, incidence angle: 0.16°) at SPring-8 BL15XU and BL24XU for comparison with those measured in laboratory. The obtained profile data were similar to those measured in our laboratory.

The crystallinity of *it*.PP substrates was calculated using the literature method reported by Weidinger and Hermans.[58]

Atomic force microscopy (AFM) measurement

To investigate the surface morphology of *it*.PP substrates after primer treatment, we performed AFM measurements on an E-sweep (SII nanotechnology Co. Ltd.) with a silicon cantilever (tip size: 10 nm, SII nanotechnology Co. Ltd.). The scanning area was 5 μm × 5 μm.

Contact angle measurement

The surface properties of *it*.PP substrates were examined by measuring static contact angles of CA droplets on *it*.PP substrates before and after the primer treatments. The contact angles θ were corrected using the $\theta/2$ method, as shown in Eq. 1.

$$\theta = 2 \tan^{-1}(2H/R) \qquad (1)$$

where R is the diameter of the contact area of the CA droplet and substrate, and H is the height of the droplet.

Interaction between cobalt primers and CA adhesive

We evaluated the interaction between the nitrile substituent of CA and cobalt complexes in toluene solution using the Raman scattering spectroscopy. We employed the ethyl 2-cyano-2-methylpropionate (CA model) as an alternative to the CA adhesive. After dissolving 0.10 mmol $Co(acac)_2$ or $Co(acac)_3$ into 20 mL toluene at 60 °C, we added 1.8 mmol CA model and the solutions were stirred for 24 h. For the Raman scattering measurements, we measured the drops of the solution covered by cover slips on the microscope slides. We observed a shift of the nitrile substituent band around 2247 cm^{-1}.

Energy dispersive X-ray spectrometry in scanning transmission electron microscopy (STEM–EDX)

We performed STEM using a TECNAI Osiris (FEI Company, Hillsboro, OR, USA) scanning transmission electron microscope equipped with four windowless silicon drift EDX detectors, which were placed symmetrically around the optical axis near the specimen area. This EDX system (Super-X) significantly enhances the EDX detection sensitivity, particularly for light elements, which enables us to rapidly detect small amounts of the elements in polymer materials. Thin

sections were prepared for the STEM process by ultra-microtoming with a diamond knife at room temperature with a preset thickness of 70 nm after they were embedded in light-curable resin (D-800, Toagosei Co., Ltd.). The sections were then placed on a copper grid covered with lacey carbon film. All the observation were performed at an accelerating voltage of 200 kV. The spatial resolution is <10 nm.[59–61]

Results and Discussion

We evaluated the effect of cobalt complex primers on the adhesive properties of *it*.PP substrates. Table 1 shows the T-peel strength of the *it*.PP/CA/*it*.PP adhered specimens with no primer treatment, as well as with $Co(acac)_2$ and $Co(acac)_3$ primer treatments. Without any primer treatment, the adhesive strength was lower than 1.0 N/cm. After applying the $Co(acac)_3$ primer, there was a negligible change in the strength, whereas in the case of $Co(acac)_2$ primer, the T-peel strength was increased drastically to more than 30 N/cm. The specimens with non- and $Co(acac)_3$-primer treatments were peeled at their interface, while the one with the $Co(acac)_2$ primer was fractured in the adhesive layer. Therefore, a clear primer effect was observed for only $Co(acac)_2$ on *it*.PP substrate. For a detailed investigation on the effect of primer on the adhesive properties, various measurements were employed from several perspectives such as primers, adhesive, the *it*.PP surface and the *it*.PP/CA interphase.

Table 1. T-peel strength of adhered *it*.PP/CA/*it*.PP specimens with non-, $Co(acac)_2$ and $Co(acac)_3$ treatment.

Applied primer	T-peel strength N/cm
Non	0.63 ±0.1
$Co(acac)_2$	32 ±3.2
$Co(acac)_3$	0.60 ±0.1

The curing velocity of the CA adhesive was evaluated by Raman scattering spectroscopy. The CA curing led to the disappearance of the band at 1612 cm^{-1}, which originated from the C=C double bond vibration shown in Figure S4 in the Supplementary material. Figure 1 shows the time

dependence of band intensities at 1612 cm^{-1} in the Raman scattering spectra of the CA adhesive on the non- or primer-applied *it*.PP substrates. The spectra of CA adhesive on the $Co(acac)_3$ primer-treated *it*.PP substrate disappeared for more than an hour. This behavior corresponded to that of the CA on the non-treated *it*.PP substrate. However, the band intensity of the CA adhesive on the $Co(acac)_2$ primer-treated *it*.PP was immediately decreased. This means that the CA curing on *it*.PP after applying $Co(acac)_2$ primer was rapidly completed. In addition, Figure S5 in the Supplementary material shows the optical images of the CA solution in toluene including the cases with no primer, $Co(acac)_2$ and $Co(acac)_3$. Only the CA solution, which included the $Co(acac)_2$ primer was gelated immediately after adding CA into the primer solution. From the GPC analysis, the molecular weights of their CA adhesives after polymerization were similar as shown in Table S1 in the Supplementary material. These results indicate that the $Co(acac)_2$ primer accelerated the anion polymerization of CA adhesives, but it had no influence on the molecular weight after polymerization.

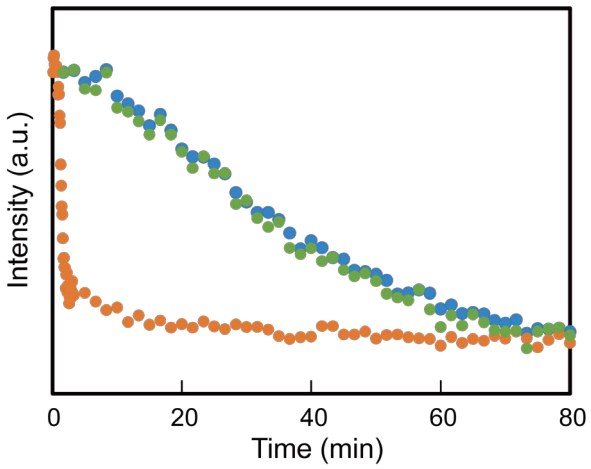

Figure 1. Intensity of Raman scattering band at 1612 cm^{-1} for CA (blue), CA+$Co(acac)_2$ (orange) and CA+$Co(acac)_3$ (green) after starting CA adhesive curing.

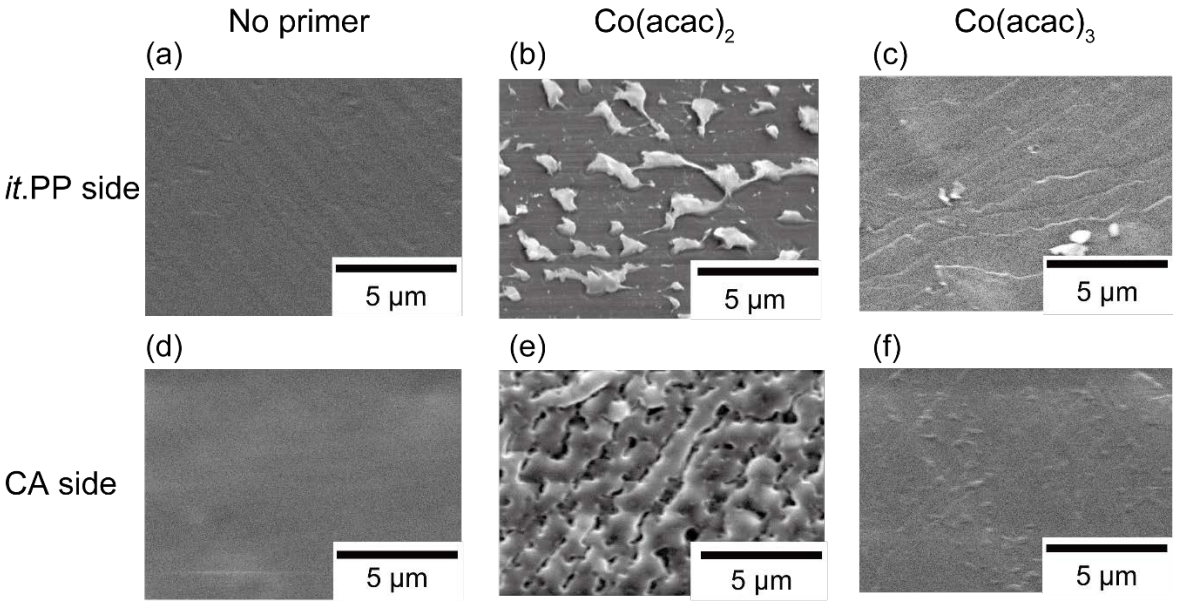

Figure 2. SEM images of the peeled surfaces of adhesive specimens of *it.*PP side with (a) no treatment, (b) $Co(acac)_2$ and (c) $Co(acac)_3$ treatments. (d) (e) and (f) represent the results of the CA side with (d) no treatment, (e) $Co(acac)_2$ and (f) $Co(acac)_3$ treatment.

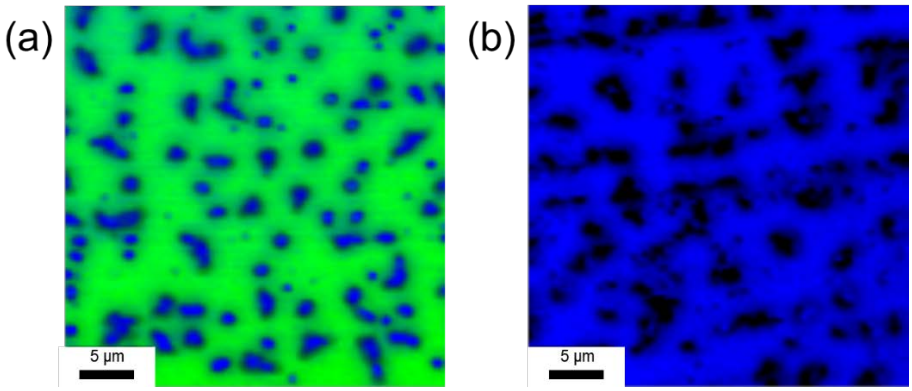

Figure 3. 2D mapping images of Raman scattering of the peeled surfaces of (a) *it.*PP substrate side and (b) CA adhesive side with $Co(acac)_2$ treatment. Green areas represent the mapping of the band at 812 cm^{-1} originated from the *it.*PP substrate and the blue ones were at 2247 cm^{-1} and originated from the CA adhesive.

The fracture mode under the T-peel test was investigated using SEM images and 2D mapping images obtained by Raman scattering. Figures 2 and 3 respectively show SEM images and 2D mapping images of Raman scattering of the surface after the peeling test. The peeled surfaces without any treatment and with the $Co(acac)_3$ primer-treatment were smooth. The peeled surface of the adhered specimen after applying the $Co(acac)_2$ primer showed significant roughness. From the measurements of the peeled surface obtained by Raman spectroscopy, the CA adhesive component was observed in the surface of the *it.*PP side. The results show that the adhered specimen after applying the $Co(acac)_2$ primer was fractured both in the adhesive layer and at the interface under the T-peel test.

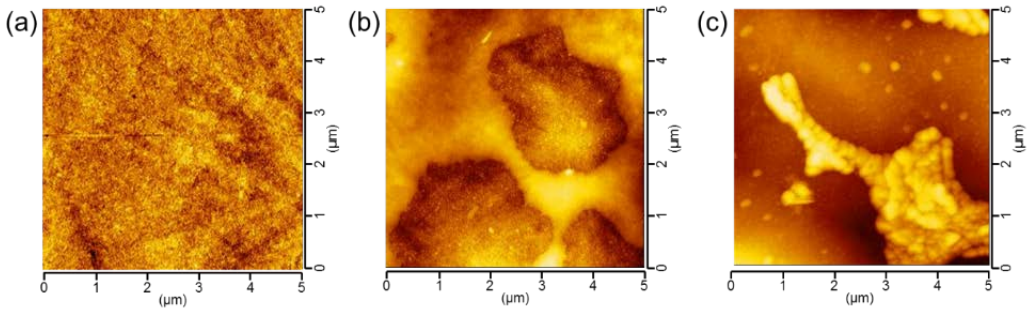

Figure 4. AFM height images of the surface of (a) *it.*PP, (b) *it.*PP after applying $Co(acac)_2$ and (c) *it.*PP after applying $Co(acac)_3$.

The surface morphologies of *it.*PP substrates after primer treatments were evaluated by performing atomic force microscopy (AFM) measurements. Their height topological geometries are shown in Figure 4. After $Co(acac)_2$ primer treatment, the cratered surface of *it.*PP emerged, while at the surface of *it.*PP after applying the $Co(acac)_3$ primer, an aggregation of the $Co(acac)_3$ complex was observed. The depth of the crater after applying the $Co(acac)_2$ primer was of the

order of several tens of nanometers. From these observations, we confirmed that $Co(acac)_2$ was well-spread on *it.*PP substrates compared with $Co(acac)_3$.

To investigate the interaction between *it.*PP and CA adhesive, we measured the contact angles of CA droplets on non-applied *it.*PP as well as *it.*PP with $Co(acac)_2$ and $Co(acac)_3$ primer treatment. Their static contact angles are described in Table 2. The contact angle of CA on the non-treated *it.*PP was 38.7°. The results obtained for the $Co(acac)_3$ primer-applied *it.*PP agreed relatively well with~~to~~ the non-applied one. However, the contact angle on *it.*PP with $Co(acac)_2$ primer treatment was drastically decreased to 15.4°. These suggested that the $Co(acac)_2$ primer modified the surface property of *it.*PP and enhanced the affinity of CA to *it.*PP. After the curing of the CA droplets, the contact angles of CA on all the *it.*PP substrates remained. Therefore, the effect of CA curing under contact angle measurements was negligible.

Table 2. Static contact angles of CA droplets on *it.*PP substrates

Applied primer	Static contact angle of CA
None	38.7° ± 0.7°
$Co(acac)_2$	15.4° ± 1.2°
$Co(acac)_3$	32.6° ± 1.6°

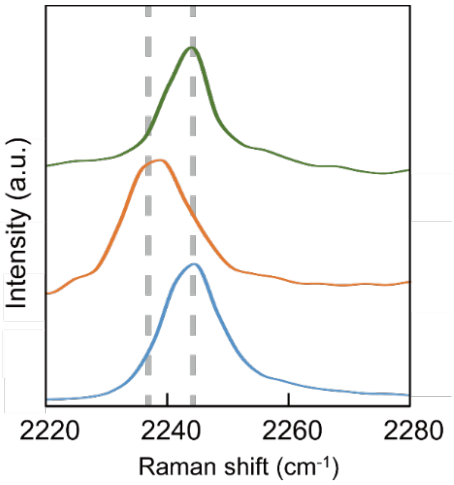

Figure 5. Expanded Raman scattering spectra around the CN vibration band of the CA model (bottom, blue), CA model+$Co(acac)_2$ (middle, orange) and CA model+$Co(acac)_3$ (top, green).

To obtain spectroscopic analyses of the interaction between the CA adhesive and cobalt primers, we measured the Raman scattering of the CA model compound and primers in solution states. We employed ethyl 2-cyano-2-methylpropionate (CA model) as a model of the CA adhesive. In Raman scattering spectroscopy, the C≡N triple-bond stretching vibration band of the CA model was detected at around 2245 cm^{-1}. As shown in Figure 5, the C≡N vibration band of the CA model was shifted by adding $Co(acac)_2$ primer compared to that of only the CA model. In contrast, the C≡N vibration band in the $Co(acac)_3$ primer/CA model solution remained unchanged. Because the $Co(acac)_3$ primer had no vacant orbitals but $Co(acac)_2$ had two coordination sites, the CA model coordinated to only the $Co(acac)_2$ primer and the Raman band was shifted. This indicated that only the $Co(acac)_2$ primer, which was coordinated by the CA adhesive,[62,63] accelerated the curing of the CA adhesive and increased the affinity for the CA adhesive.

In previous section, we discussed the significant primer effect of $Co(acac)_2$. We focused on the primer structure of the *it*.PP surface and measured the grazing-incidence (GI) X-ray diffraction.

The critical angle α_c of *it*.PP was 0.149°. Therefore, for the incidence angle of the X-ray beam α, we used 0.10°. Figure 6 shows the GI X-ray diffraction profiles of non-applied *it*.PP and *it*.PP after applying $Co(acac)_2$ and $Co(acac)_3$ primers. The measurements were carried out with both the out-of-plane and in-plane geometries. The observed crystal modification of *it*.PP was the most conventional α-form. In the out-of-plane X-ray diffraction profiles of *it*.PP after $Co(acac)_2$ and $Co(acac)_3$ primer treatment, diffraction peaks appeared at 8.4° and 11.0°, respectively. The diffraction peak at 8.4° originated from the (100) plane of the tetranuclear complex $[Co(acac)_2]_4$ [64] and that at 11.0° was from the (002) plane of $Co(acac)_3$.[65] Both the diffraction peaks were undetectable in the in-plane measurements. This means that these two lattice planes were oriented in the direction perpendicular to the *it*.PP substrates, as shown in Figure 7. The primers on the *it*.PP surface crystalized with their metal complex structure, and were oriented to the substrates. It has been reported that as opposed to $Co(acac)_3$ complexes, $[Co(acac)_2]_4$ complexes possessed coordination sites. On the *it*.PP substrates, the coordination sites of the $[Co(acac)_2]_4$ complex were directed upward, where vacant orbitals were exposed to the surface. Thus, it is considered that the CN group of CA can easily coordinate to the vacant orbital, which is expected to result in a large primer effect of $Co(acac)_2$.

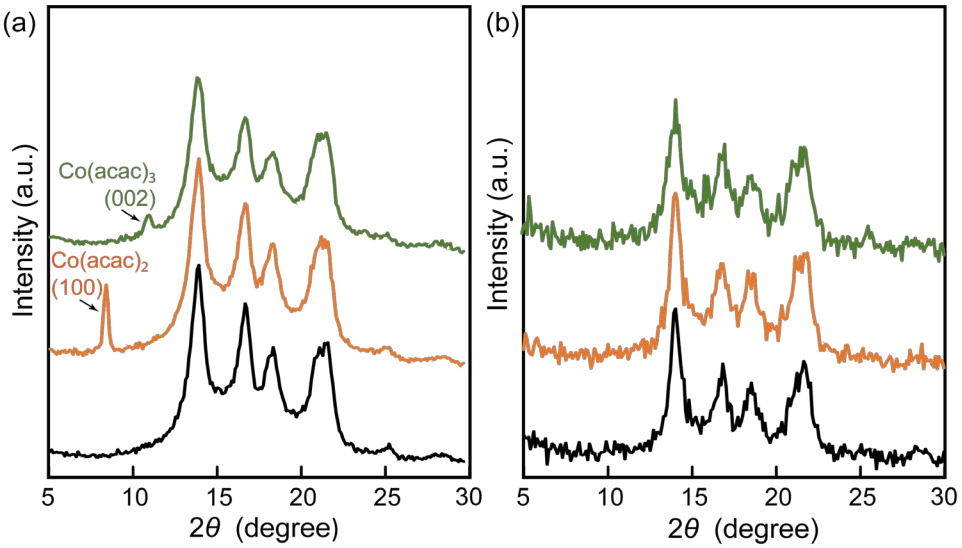

Figure 6. GI X-ray diffraction profiles of *it.*PP (bottom, black), *it.*PP after applying $Co(acac)_2$ (middle, orange) and *it.*PP after applying $Co(acac)_3$ (top, green) measured with (a) out-of-plane and (b) in-plane geometries.

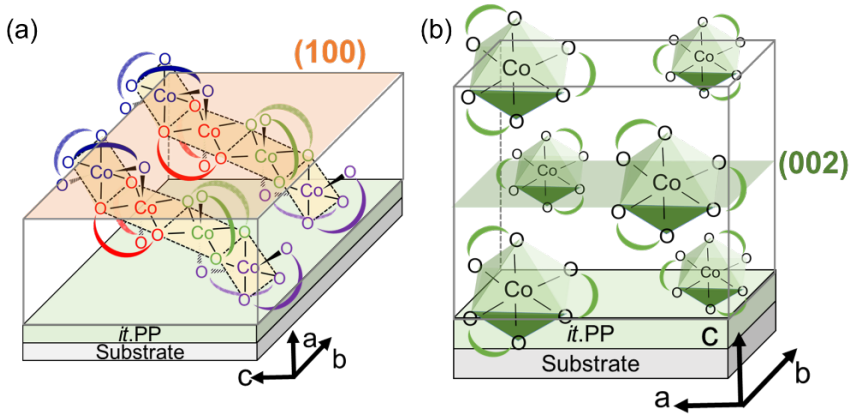

Figure 7. Schematic illustration of $Co(acac)_2$ and $Co(acac)_3$ orientation on *it.*PP.

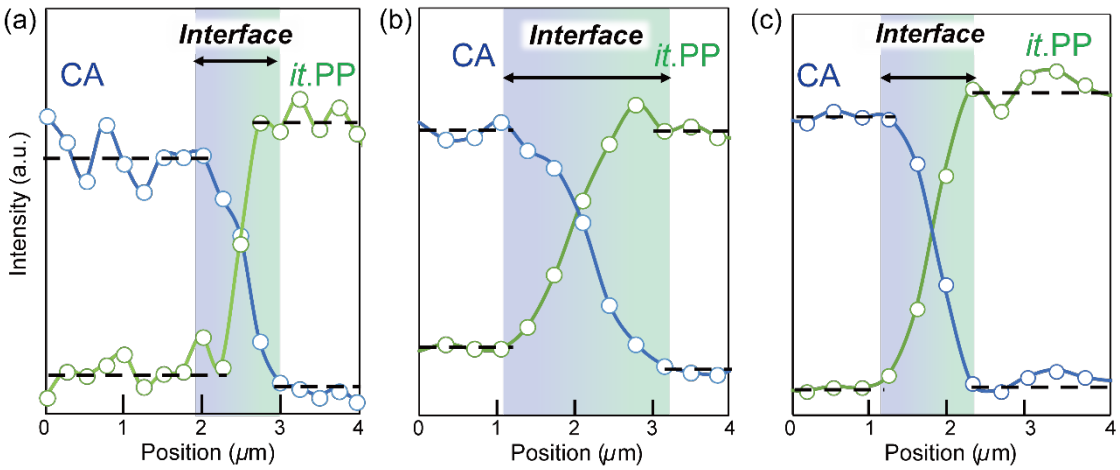

Figure 8. Profiles of Raman scattering bands at 2247 cm^{-1} (blue) and 812 cm^{-1} (green) across the *it*.PP/CA interphase with (a) no primer, (b) $Co(acac)_2$ and (c) $Co(acac)_3$.

In the above discussion, the interactions between *it*.PP substrates, cobalt primers and CA adhesive before adhesion were described. Next, to determine the effect of primers on the adhesive strength, we investigated the interphase of adhered specimens using nano-Raman scattering microscopy. The Raman scattering spectrum of each component, *it*.PP and cured CA adhesive, is shown in Figure S6 in the Supplementary material. The cross section of the adhered *it*.PP/CA sample without primer treatment was measured across the adhesion interphase. The measuring points were swept from the CA adhesive to the *it*.PP substrate with increments of 350 nm. Figure S8 in the Supplementary material shows the obtained spectra. The bands that originated from CA adhesives were gradually decreased, and the bands of *it*.PP were increased. For example, the C≡N vibration band of CA adhesive at 2247 cm^{-1} was decreased, and the band of the *it*.PP substrate at 812 cm^{-1} increased. The integrated intensities of both bands were plotted as shown in Figure 8 (a). The integrated intensity of the band of the CA adhesive and *it*.PP were inverted relative to each other at the adhesion interphase. In this study, the inverting region was defined as the interfacial thickness. Table 3 shows the interfacial thickness of adhered *it*.PP/CA samples without any primer

treatment and with $Co(acac)_2$ and $Co(acac)_3$ primer treatment. The interfacial thickness with $Co(acac)_3$ primer treatment was similar to that without any primer treatment, while the thickness after applying the $Co(acac)_2$ primer was twice as large as the non-treated one. These results agreed with their tendency of adhesive strength.[51,66]

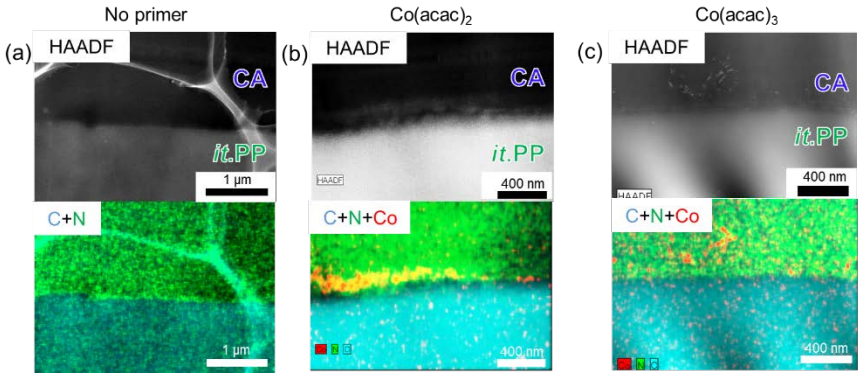

Figure 9. STEM-EDX mapping images around the *it*.PP/CA interphase with (a) non-treatment, (b) $Co(acac)_2$ treatment and (c) $Co(acac)_3$ treatment. Top : HAADF images. Bottom : element mapping images (carbon : blue, nitrogen : green, cobalt : red).

Table 3. Interfacial thickness of *it*.PP/CA estimated by Raman scattering and STEM-EDX measurements.

Applied primer	Interfacial thickness		
	Nano-Raman (μm)	STEM-EDX (nm)	
		N	C
None	1.2±0.4	40	140
$Co(acac)_2$	2.5±0.7	150	200
$Co(acac)_3$	1.4±0.6	80	120

For an in-depth investigation into the adhesive interfacial thickness, we evaluated the adhesion interphases with STEM-EDX. Figure 9 shows the high-angle annular dark-field (HAADF) images and EDX elemental maps of carbon, nitrogen and cobalt elements in the region around the interphase of *it.*PP/CA without any primer treatment as well as with $Co(acac)_2$ and $Co(acac)_3$ primer treatment. In all of the adhered specimens, the interphases of *it.*PP/CA were observed clearly. In addition, the interphase after applying $Co(acac)_2$ primer, as opposed to the $Co(acac)_3$ primer, included the thin layer containing the cobalt element. This indicated that the $Co(acac)_2$ primer was localized at the interphase and enhanced the adhesive strength effectively, as shown in Figure S9 (d) in the Supplementary material. In contrast, the $Co(acac)_3$ primer on the *it.*PP substrate was eluted and diffused to the CA side owing to the slow polymerization of CA in Figure S9 (e) in the Supplementary material. Figure S10 in the Supplementary material shows the profile of the element abundance ratios of nitrogen and carbon across the interphase with $Co(acac)_2$ and $Co(acac)_3$ primer treatment. The inversions of the elemental ratios at the interphase corresponded to the case of the nano-Raman scattering analyses. The interfacial thickness is shown in Table 3. The thickness of the interphase after applying $Co(acac)_2$ primer was larger than that after $Co(acac)_3$ primer treatment. While these results are reasonable, the absolute values of the interfacial thickness obtained by STEM-EDX measurements were significantly different from that obtained by nano-Raman scattering spectroscopy. This difference was attributed to the spatial resolution of the instruments. Therefore, to obtain a complete understanding about the adhesion interphase, there is a need for a larger contribution to the interfacial analyses. This implies that the primer effect of $Co(acac)_2$ was inspired by the curing acceleration of CA adhesive, the improvement of the affinity between the *it.*PP and CA adhesive and the larger interfacial thickness of *it.*PP/CA. In particular,

these spatial interfacial regions can be referred to not as an interface, but as an “interphase”, which controls the adhesive properties.

From the above analyses of the interfacial thickness, it is shown that the mutual diffusion was one of the key factors affecting the high adhesion. Therefore, we measured the adhesive strength of CA adhesives to *it*.PP substrates with various surface crystallinities. The crystallinities were controlled by the annealing temperature and estimated using the GI X-ray diffraction profiles shown in Figure S11 in the Supplementary material. As the annealing temperature increased, the crystallinities increased, as shown in Table S2 in the Supplementary material. The adhesive strength of *it*.PP substrates with larger crystallinities decreased even after $Co(acac)_2$ primer treatment in Figure 10. This may be because the crystalline regions of *it*.PP with higher density and limited molecular mobility inhibit the mutual diffusion of *it*.PP, $Co(acac)_2$ primer and CA adhesive relative to the non-crystalline region.

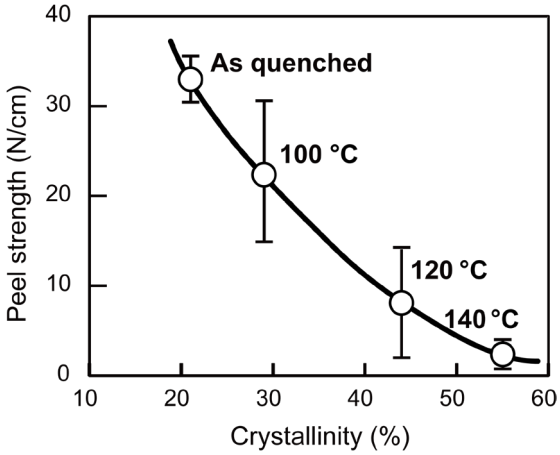

Figure 10. T-peel strength of *it*.PP/CA/*it*.PP with various surface crystallinity of *it*.PP substrates.

CONCLUSIONS

In this study, we investigated the effect of cobalt complex primers on the adhesive properties of *it*.PP substrate and CA adhesive from the perspectives of molecular morphology and chemical interaction. In particular, $Co(acac)_2$ complex, as opposed to $Co(acac)_3$, improved the adhesive property of *it*.PP effectively. Based on the various measurements results obtained, it was shown that the electronic state, molecular interaction and diffusivity of $Co(acac)_2$ resulted in a high curing velocity, high affinity between the adhesive and substrate, large interfacial thickness, and subsequently a high adhesive strength. Here, we evaluated the interfacial thickness using nano-Raman scattering spectroscopy and STEM-EDX. The results obtained by both measurement methods were in agreement with each other. In addition, we varied the adhesive strength using the surface crystallinity of *it*.PP substrates, which confirmed the effect of the mutual diffusion on the adhesive strength.

ASSOCIATED CONTENT

Supplementary Material.

This material is available free of charge via the Internet at http://

AUTHOR INFORMATION

Corresponding Author

*(T.N.) E-mail: tnishino@kobe-u.ac.jp

Funding Sources

This work was partially supported by a Grant-in-Aid for Scientific Research on Innovative Areas “New Polymeric Materials Based on Element-Blocks (No.2401)” (24102009) of The Ministry of Education, Culture, Sports, Science, and Technology, Japan.

Notes

The authors declare no competing financial interest.

ACKNOWLEDGEMENT

The synchrotron radiation experiments were performed at the BL15XU, BL24XU of SPring-8 with the approval of the National Institute for Materials Science (NIMS) and the Japan Synchrotron Radiation Research Institute (JASRI) (Proposal No. 2011B3255, 2012A4803, 2012B4803). We would like to thank Editage (www.editage.jp) for English language editing.

REFERENCES

[1] K. Ziegler, Folgen und Werdegang einer Erfindung Nobel-Vortrag, Angew. Chemie. 76 (1964) 545–553. doi:10.1002/ange.19640761302.

[2] K. Ziegler, E. Holzkamp, H. Breil, H. Martin, Das Mülheimer Normaldruck-Polyäthylen-Verfahren, Angew. Chemie. 67 (1955) 541–547. doi:10.1002/ange.19550671902.

[3] N. Pasquini, ed., Polypropylene Handbook, 2nd Editio, Hanser Publications, 2005. https://books.google.co.jp/books/about/Polypropylene_Handbook.html?id=SP7bwXwlvPAC&redir_esc=y.

[4] G.W. Coates, Precise Control of Polyolefin Stereochemistry Using Single-Site Metal Catalysts, Chem. Rev. 100 (2000) 1223–1252. doi:10.1021/cr990286u.

[5] G.J. Domski, J.M. Rose, G.W. Coates, A.D. Bolig, M. Brookhart, Living alkene polymerization: New methods for the precision synthesis of polyolefins, Prog. Polym. Sci. 32 (2007) 30–92. doi:http://dx.doi.org/10.1016/j.progpolymsci.2006.11.001.

[6] G.W. Coates, P.D. Hustad, S. Reinartz, Catalysts for the Living Insertion Polymerization of Alkenes: Access to New Polyolefin Architectures Using Ziegler–Natta Chemistry, Angew. Chemie Int. Ed. 41 (2002) 2236–2257. doi:10.1002/1521-3773(20020703)41:13<2236::AID-ANIE2236>3.0.CO;2-3.

[7] T.R. Younkin, E.F. Connor, J.I. Henderson, S.K. Friedrich, R.H. Grubbs, D.A. Bansleben, Neutral, Single-Component Nickel (II) Polyolefin Catalysts That Tolerate Heteroatoms, Science 287 (2000) 460 LP-462. http://science.sciencemag.org/content/287/5452/460.abstract.

[8] H. Karian, Handbook of polypropylene and polypropylene composites, Revised and Expanded, 2003. doi:10.1017/CBO9781107415324.004.

[9] F. Ide, A. Hasegawa, Studies on polymer blend of nylon 6 and polypropylene or nylon 6 and polystyrene using the reaction of polymer, J. Appl. Polym. Sci. 18 (1974) 963–974. doi:10.1002/app.1974.070180402.

[10] U. Sundararaj, C.W. Macosko, Drop Breakup and Coalescence in Polymer Blends: The Effects of Concentration and Compatibilization, Macromolecules. 28 (1995) 2647–2657. doi:10.1021/ma00112a009.

[11] P. Santos, S.H. Pezzin, Mechanical properties of polypropylene reinforced with recycled-pet fibres, J. Mater. Process. Technol. 143 (2003) 517–520. doi:http://dx.doi.org/10.1016/S0924-0136(03)00391-1.

[12] D.R. Paul, L.M. Robeson, Polymer nanotechnology: Nanocomposites, Polymer 49 (2008) 3187–3204. doi:http://dx.doi.org/10.1016/j.polymer.2008.04.017.

[13] J.N. Coleman, U. Khan, W.J. Blau, Y.K. Gun'ko, Small but strong: A review of the mechanical properties of carbon nanotube–polymer composites, Carbon N. Y. 44 (2006) 1624–1652. doi:http://dx.doi.org/10.1016/j.carbon.2006.02.038.

[14] S. Panthapulakkal, M. Sain, Injection-molded short hemp fiber/glass fiber-reinforced polypropylene hybrid composites—Mechanical, water absorption and thermal properties, J. Appl. Polym. Sci. 103 (2007) 2432–2441. doi:10.1002/app.25486.

[15] J.M. Garcés, D.J. Moll, J. Bicerano, R. Fibiger, D.G. McLeod, Polymeric Nanocomposites for Automotive Applications, Adv. Mater. 12 (2000) 1835–1839. doi:10.1002/1521-4095(200012)12:23<1835::AID-ADMA1835>3.0.CO;2-T.

[16] F. Awaja, M. Gilbert, G. Kelly, B. Fox, P.J. Pigram, Adhesion of polymers, Prog. Polym. Sci. 34 (2009) 948–968. doi:http://dx.doi.org/10.1016/j.progpolymsci.2009.04.007.

[17] D.M. Brewis, D. Briggs, Adhesion to polyethylene and polypropylene, Polymer 22 (1981) 7–16. doi:http://dx.doi.org/10.1016/0032-3861(81)90068-9.

[18] K. Kimura, Adhesives for Polyolefine Resins, J. Adhes. Soc. Japan Adhes. 23 (1987) 443–448.

[19] E.M. Liston, L. Martinu, M.R. Wertheimer, Plasma surface modification of polymers for improved adhesion: a critical review, J. Adhes. Sci. Technol. 7 (1993) 1091–1127. doi:10.1163/156856193X00600.

[20] M. Noeske, J. Degenhardt, S. Strudthoff, U. Lommatzsch, Plasma jet treatment of five polymers at atmospheric pressure: surface modifications and the relevance for adhesion, Int. J. Adhes. Adhes. 24 (2004) 171–177. doi:http://dx.doi.org/10.1016/j.ijadhadh.2003.09.006.

[21] R. Dorai and M.J. Kushner, A model for plasma modification of polypropylene using atmospheric pressure discharges, J. Phys. D. Appl. Phys. 36 (2003) 666. http://stacks.iop.org/0022-3727/36/i=6/a=309.

[22] D. Hegemann, H. Brunner, C. Oehr, Plasma treatment of polymers for surface and adhesion improvement, Nucl. Instruments Methods Phys. Res. Sect. B Beam Interact. with Mater. Atoms. 208 (2003) 281–286. doi:http://dx.doi.org/10.1016/S0168-583X(03)00644-X.

[23] I. Sutherland, D.M. Brewis, R.J. Health, E. Sheng, Modification of polypropylene surfaces by flame treatment, Surf. Interface Anal. 17 (1991) 507–510. doi:10.1002/sia.740170717.

[24] N. Encinas, J. Abenojar, M.A. Martínez, Development of improved polypropylene adhesive bonding by abrasion and atmospheric plasma surface modifications, Int. J. Adhes. Adhes. 33 (2012) 1–6. doi:http://dx.doi.org/10.1016/j.ijadhadh.2011.10.002.

[25] V. Goel, U. Beginn, A. Mourran, M. Möller, “Quat-Primer” Polymers Bearing Cationic and Reactive Groups: Synthesis, Characterization, and Application, Macromolecules. 41 (2008) 8187–8197. doi:10.1021/ma801064e.

[26] P. Klemarczyk, The isolation of a zwitterionic initiating species for ethyl cyanoacrylate (ECA) polymerization and the identification of the reaction products between 1°, 2°, and 3° amines with ECA, Polymer 42 (2001) 2837–2848. doi:http://dx.doi.org/10.1016/S0032-3861(00)00618-2.

[27] Y. Okamoto, P.T. Klemarczyk, Primers for Bonding Polyolefin Substrates with Alkyl Cyanoacrylate Adhesive, J. Adhes. 40 (1993) 81–91. doi:10.1080/00218469308031275.

[28] J. Yang, A. Garton, Primers for adhesive bonding to polyolefins, J. Appl. Polym. Sci. 48 (1993) 359–370. doi:10.1002/app.1993.070480220.

[29] V. Lenaerts, P. Couvreur, D. Christiaens-Leyh, E. Joiris, M. Roland, B. Rollman, P. Speiser, Degradation of poly (isobutyl cyanoacrylate) nanoparticles, Biomaterials. 5 (1984) 65–68. doi:http://dx.doi.org/10.1016/0142-9612(84)90002-4.

[30] J.I. Lim, Y.-K. Lee, J.-S. Shin, K.-J. Lim, Cyanoacrylate adhesives curable to flexible polymeric materials by poly(l-lactide-co-ε-caprolactone), Mater. Lett. 64 (2010) 2438–2440. doi:http://dx.doi.org/10.1016/j.matlet.2010.07.064.

[31] M.F. Sonnenschein, S.P. Webb, P.E. Kastl, D.J. Arriola, B.L. Wendt, D.R. Harrington, N.G. Rondan, Mechanism of Trialkylborane Promoted Adhesion to Low Surface Energy Plastics, Macromolecules. 37 (2004) 7974–7978. doi:10.1021/ma040095f.

[32] M.F. Sonnenschein, S.P. Webb, O.D. Redwine, B.L. Wendt, N.G. Rondan, Physical and Chemical Probes of the Bond Strength between Trialkylboranes and Amines and Their

Utility as Stabilized Free Radical Polymerization Catalysts, Macromolecules. 39 (2006) 2507–2513. doi:10.1021/ma060268w.

[33] T.E. Gentle, R.G. Schmidt, B.M. Naasz, A.J. Gellman, T.M. Gentle, Organofunctional silanes as adhesion promoters: direct characterization of the polymer/silane interphase, J. Adhes. Sci. Technol. 6 (1992) 307–316. doi:10.1163/156856192X00359.

[34] L.H. Sharpe, The Interphase in Adhesion, J. Adhes. 4 (1972) 51–64. doi:10.1080/00218467208072210.

[35] K. Kendall, Adhesion: Molecules and Mechanics, Science 263 (1994) 1720–1725. doi:10.1126/science.263.5154.1720.

[36] A. Hartwig, R. Meissner, C. Merten, P. Schiffels, P. Wand, I. Grunwald, Mutual Influence Between Adhesion and Molecular Conformation: Molecular Geometry is a Key Issue in Interphase Formation, J. Adhes. 89 (2013) 77–95. doi:10.1080/00218464.2013.731363.

[37] G. Tao, A. Gong, J. Lu, H.-J. Sue, D.E. Bergbreiter, Surface Functionalized Polypropylene: Synthesis, Characterization, and Adhesion Properties, Macromolecules. 34 (2001) 7672–7679. doi:10.1021/ma010941b.

[38] J. Friedrich, G. Kühn, R. Mix, A. Fritz, A. Schönhals, Polymer surface modification with monofunctional groups of variable types and densities, J. Adhes. Sci. Technol. 17 (2003) 1591–1617. doi:10.1163/156856103322396695.

[39] N.M. Alves, C. Picart, J.F. Mano, Self Assembling and Crosslinking of Polyelectrolyte Multilayer Films of Chitosan and Alginate Studied by QCM and IR Spectroscopy, Macromol. Biosci. 9 (2009) 776–785. doi:10.1002/mabi.200800336.

[40] K. Adamsons, Chemical surface characterization and depth profiling of automotive coating systems, Prog. Polym. Sci. 25 (2000) 1363–1409. doi:http://dx.doi.org/10.1016/S0079-6700(00)00031-9.

[41] L. Li, C.-T. Lin, SEM-EDS Investigations of Self-Phosphating Coatings, Ind. Eng. Chem. Res. 33 (1994) 3241–3246. doi:10.1021/ie00036a045.

[42] J.T. Marchesi, H.D. Keith, A. Garton, Adhesion to Sodium Naphthalenide Treated Fluoropolymers. Part III. Mechanism of Adhesion, J. Adhes. 39 (1992) 185–205. doi:10.1080/00218469208030462.

[43] S. Wu, E.T. Kang, K.G. Neoh, H.S. Han, K.L. Tan, Surface Modification of Poly(tetrafluoroethylene) Films by Graft Copolymerization for Adhesion Improvement with Evaporated Copper, Macromolecules. 32 (1999) 186–193. doi:10.1021/ma9803133.

[44] E. Boucher, J.P. Folkers, H. Hervet, L. Léger, C. Creton, Effects of the Formation of Copolymer on the Interfacial Adhesion between Semicrystalline Polymers, Macromolecules. 29 (1996) 774–782. doi:10.1021/ma9509422.

[45] J.T. Koberstein, Molecular design of functional polymer surfaces, J. Polym. Sci. Part B Polym. Phys. 42 (2004) 2942–2956. doi:10.1002/polb.20157.

[46] M. Bou, J.M. Martin, T. Le Mogne, L. Vovelle, Chemistry of the interface between aluminium and polyethyleneterephthalate by XPS, Appl. Surf. Sci. 47 (1991) 149–161. doi:http://dx.doi.org/10.1016/0169-4332(91)90029-J.

[47] D. Wolany, T. Fladung, L. Duda, J.W. Lee, T. Gantenfort, L. Wiedmann, A. Benninghoven, Combined ToF-SIMS/XPS study of plasma modification and metallization of polyimide, Surf. Interface Anal. 27 (1999) 609–617. doi:10.1002/(SICI)1096-9918(199907)27:7<609::AID-SIA523>3.0.CO;2-#.

[48] H. Aoki, S. Tanaka, S. Ito, M. Yamamoto, Nanometric Inhomogeneity of Polymer Network Investigated by Scanning Near-Field Optical Microscopy, Macromolecules. 33 (2000) 9650–9656. doi:10.1021/ma001274+.

[49] L.G. Parratt, Surface Studies of Solids by Total Reflection of X-Rays, Phys. Rev. 95 (1954) 359–369. doi:10.1103/PhysRev.95.359.

[50] Y.R. Shen, Wave mixing spectroscopy for surface studies, Solid State Commun. 102 (1997) 221–229. doi:http://dx.doi.org/10.1016/S0038-1098(96)00726-0.

[51] D. Zhang, Y.R. Shen, G.A. Somorjai, Studies of surface structures and compositions of polyethylene and polypropylene by IR+visible sum frequency vibrational spectroscopy, Chem. Phys. Lett. 281 (1997) 394–400. doi:http://dx.doi.org/10.1016/S0009-2614(97)01311-0.

[52] A. Morita, J.T. Hynes, A theoretical analysis of the sum frequency generation spectrum of the water surface, Chem. Phys. 258 (2000) 371–390. doi:http://dx.doi.org/10.1016/S0301-0104(00)00127-0.

[53] K.S. Gautam, A.D. Schwab, A. Dhinojwala, D. Zhang, S.M. Dougal, M.S. Yeganeh, Molecular Structure of Polystyrene at Air/Polymer and Solid/Polymer Interfaces, Phys. Rev. Lett. 85 (2000) 3854–3857. doi:10.1103/PhysRevLett.85.3854.

[54] C.T. Dotter, M.L. Goldman, J. Rösch, Instant Selective Arterial Occlusion with Isobutyl 2-Cyanoacrylate, Radiology. 114 (1975) 227. doi:10.1148/114.1.227.

[55] M. Arruebarrena de Báez, P.J. Hendra, M. Judkins, The Raman spectra of oriented isotactic polypropylene, Spectrochim. Acta Part A Mol. Biomol. Spectrosc. 51 (1995) 2117–2124. doi:http://dx.doi.org/10.1016/0584-8539(95)01512-1.

[56] H.G.M. Edwards, J.S. Day, Fourier transform Raman spectroscopic studies of the curing of cyanoacrylate glue, J. Raman Spectrosc. 35 (2004) 555–560. doi:10.1002/jrs.1184.

[57] T. Nishino, T. Matsumoto, K. Nakamae, Surface structure of isotactic polypropylene by X-ray diffraction, Polym. Eng. Sci. 40 (2000) 336–343. doi:10.1002/pen.11167.

[58] A. Weidinger, P.H. Hermans, On the determination of the crystalline fraction of isotactic polypropylene from x-ray diffraction, Die Makromol. Chemie. 50 (1961) 98–115. doi:10.1002/macp.1961.020500107.

[59] K. Enomoto, Y. Ichijo, M. Nakano, M. Kikuchi, A. Narumi, S. Horiuchi, S. Kawaguchi, Unique Hydrophobization and Hybridization via Direct Phase Transfer of ZrO_2 Nanoparticles from Water to Toluene Producing Highly Transparent Polystyrene and Poly(methyl methacrylate) Hybrid Bulk Materials, Macromolecules. (2017) acs.macromol.7b02155. doi:10.1021/acs.macromol.7b02155.

[60] Z. Fu, H. Wang, X. Zhao, S. Horiuchi, Y. Li, Immiscible polymer blends compatibilized with reactive hybrid nanoparticles: Morphologies and properties, Polymer 132 (2017) 353–361. doi:10.1016/j.polymer.2017.11.004.

[61] J.H. Dycus, J.S. Harris, X. Sang, C.M. Fancher, S.D. Findlay, A.A. Oni, T.T.E. Chan, C.C. Koch, J.L. Jones, L.J. Allen, D.L. Irving, J.M. Le Beau, Accurate Nanoscale Crystallography in Real-Space Using Scanning Transmission Electron Microscopy, Microsc. Microanal. 21 (2015) 946–952. doi:10.1017/S1431927615013732.

[62] J.P. Fackler, The Reaction of Pyridine with Cobalt(II) Acetylacetonate in Benzene. Evidence for a Polymeric Species, Inorg. Chem. 2 (1963) 266–270. doi:10.1021/ic50006a007.

[63] M.B. Hursthouse, M.A. Laffey, P.T. Moore, D.B. New, P.R. Raithby, P. Thornton, Crystal and molecular structures of some binuclear complexes of cobalt(II) and nickel(II) acetylacetonates with pyridines and piperidine and a refinement of the crystal and molecular structure of hexakis-(acetylacetonato)trinickel(II), J. Chem. Soc. Dalt. Trans. (1982) 307–312. doi:10.1039/DT9820000307.

[64] F.A. Cotton, R.C. Elder, Crystal Structure of Tetrameric Cobalt(II) Acetylacetonate, Inorg. Chem. 4 (1965) 1145–1151. doi:10.1021/ic50030a012.

[65] J.P. Fackler, A. Avdeef, Crystal and molecular structure of tris(2,4-pentanedionato)manganese(III), $Mn(O_2C_5H_7)_3$, a distorted complex as predicted by Jahn-Teller arguments, Inorg. Chem. 13 (1974) 1864–1875. doi:10.1021/ic50138a016.

[66] M. Kotera, Y. Urushihara, D. Izumo, T. Nishino, Interfacial structure of all-polyethylene laminate using scanning thermal microscope and nano-Raman spectroscope, Polymer 53 (2012) 1966–1971. doi:http://dx.doi.org/10.1016/j.polymer.2012.02.038.

TOC

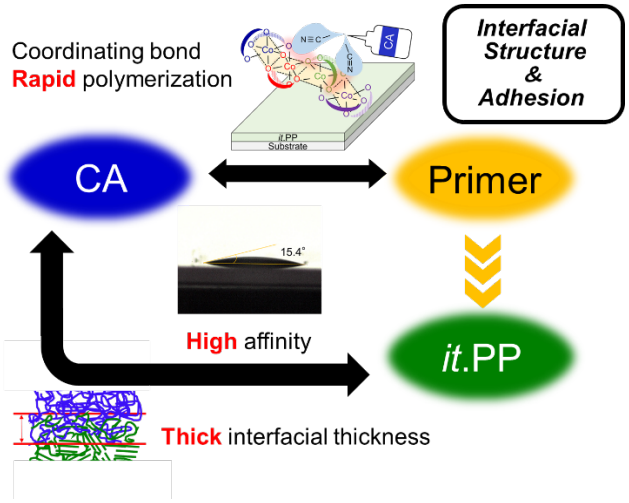
Coordinating bond
Rapid polymerization
Interfacial Structure & Adhesion
CA
Primer
15.4°
High affinity
it.PP
Thick interfacial thickness